ACS OMEGA

http://pubs.acs.org/journal/acsodf

Article

Development of a New Multiple Stimuli-Responsive Fluorescent Material Using the Minus Strategy Based on the Structure of Tetraphenyl-1,3-butadiene

Xiang Lin, Xinli Wang, Renfu Li, Zexin Wang, Wei Liu, Liwei Chen, Nannan Chen, Shitao Sun, Zhenli Li, Jinle Hao, Bin Lin, and Lijun Xie*

Cite This: *ACS Omega* 2022, 7, 10994−11001

Read Online

ACCESS | Metrics & More | Article Recommendations | Supporting Information

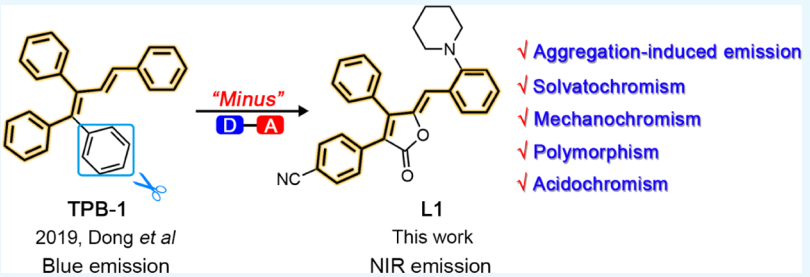

ABSTRACT: In this study, we designed and synthesized a new class of aggregation-induced emission luminogens, which was inspired and developed from the structure of tetraphenyl-1,3-butadienes derivative (TPB-1) through the minus strategy by removing one of the phenyl groups. Among them, **L1** and **L4** exhibited an aggregation-induced emission effect and multistimuli-responsive chromic behavior. Moreover, two types of single crystals of **L1** were obtained, and their different emission behaviors were elucidated clearly by analyzing the single-crystal data.

INTRODUCTION

Over the past decades, multiple stimuli-responsive (MSR) fluorescent materials have attracted tremendous interest due to their application in various areas, such as organic light-emitting diodes, organic lasers, bioimaging, security inks, and optical storage.[1−5] However, most of MSR fluorescent materials were derived by enlarging the π-system of the existing AIEgens as the main practice which could be named as a "plus strategy", such as tetraphenylethene (TPE), carbazole, quinoxaline, and others.[6−11]

The *cis*,*cis*-1,2,3,4 tetraphenylbutadiene (TPBD) and TPE were synthesized as typical MSR-active material scaffolds by Cao in 2004 and Zeng's groups in 2006.[12,13] In recent years, many TPE/TPBD types of MSR materials have been studied well using the "plus strategy". However, it demanded tedious synthetic routes with the disadvantage of high cost.[14,15] These drawbacks of traditional MSR materials drive chemists to develop much more practically obtainable MSR materials by narrowing down the original system of TPE or TPBD. It was defined as the "minus strategy". To the best of our knowledge, there are few studies using a minus strategy to develop new MSR materials.[13] Therefore, it is significant but challenging to make this strategy work.

Herein, we proposed a new strategy to construct a new kind of MSR material by removing one of the benzene rings at the 1-position of a tetraphenyl-1,3-butadiene derivative (TPB-1).[16] As shown in Scheme 1, a new series of fluorophores (**L1**−**L4**) were designed and synthesized via two synthetic steps (Scheme S1). The structures of the products obtained were fully confirmed by ^{1}H NMR, ^{13}C NMR, and HR-MS (Figures S1−S15). The relevant experimental section is shown in the Supporting Information. Impressively, **L1** and **L4** exhibited MSR properties including aggregation-induced emission (AIE) effect, reversible mechanofluochromic (MFC) behavior, and acidochromic properties. Moreover, two types of single crystals of **L1** were obtained in the toluene solvent at different temperatures. The different emission color of both the crystals was induced from different conformations and molecular packing modes elucidated clearly by analyzing the crystal data of **L1**. All this work provided a new idea for designing new MSR materials.

RESULTS AND DISCUSSION

The UV−vis absorption and fluorescence emission spectra of **L1**−**L4** in dichloromethane (DCM) are displayed in Figure S16

Received: December 7, 2021
Accepted: February 18, 2022
Published: March 28, 2022

https://doi.org/10.1021/acsomega.1c06916
ACS Omega 2022, 7, 10994−11001

Scheme 1. Molecular Structures of 4-(2-oxo-4-Phenyl-2,5-dihydrofuran-3-yl) Benzonitrile (OPBD) and L1−L4

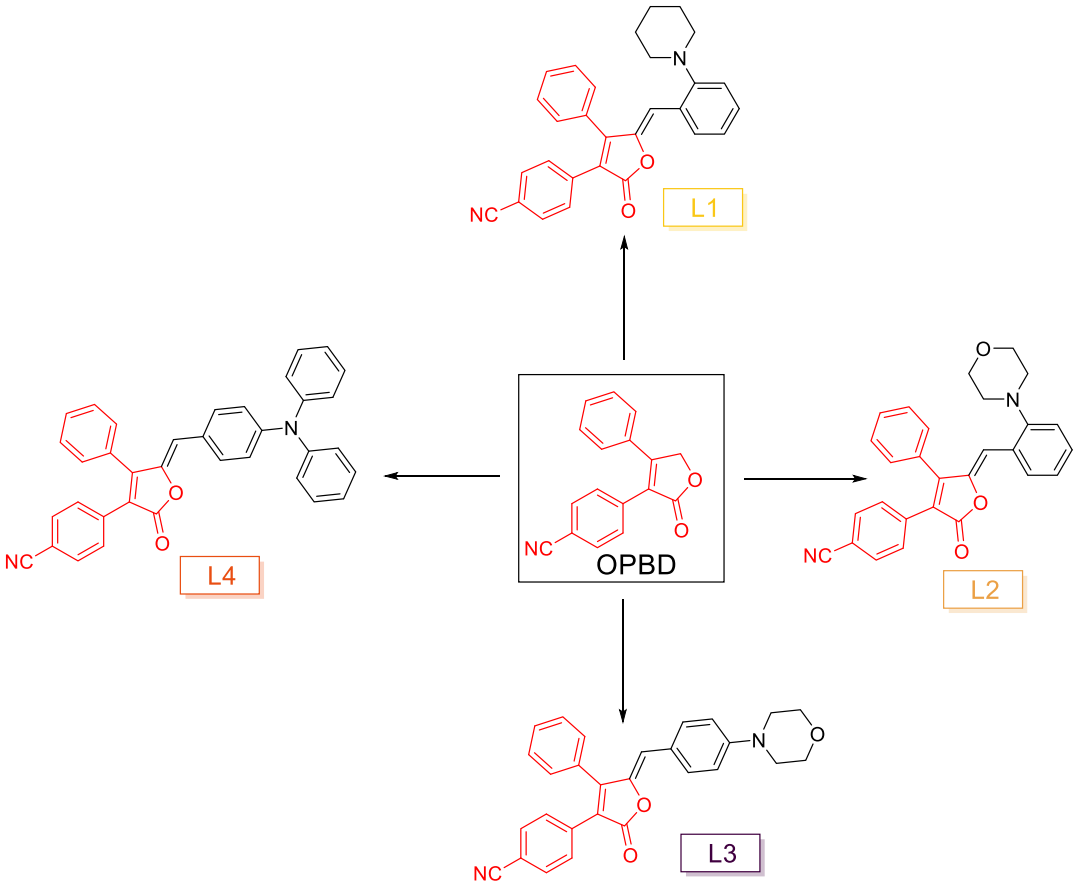

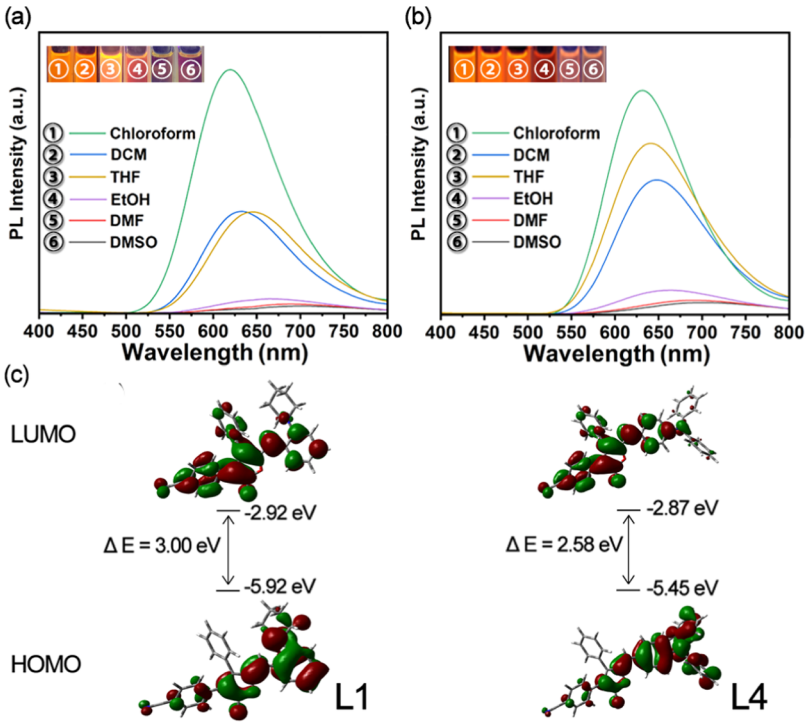

Figure 1. Emission spectra of **L1** (a) and **L4** (b) in different solvents; (c) calculation of the spatial distribution of HOMO and LUMO for **L1** and **L4**. Inset: Fluorescence images of **L1** and **L4** in different solvents under UV light (excited wavelength: 365 nm, 5×10^{-5} M).

and Table S1. Compounds **L1**−**L4** had two absorption bands. The absorption band situated at 325−375 nm could be ascribed to the localized $\pi-\pi^*$ transition. The other absorption band at the longer wavelength around 400−500 nm could be attributed

https://doi.org/10.1021/acsomega.1c06916
ACS Omega 2022, 7, 10994−11001

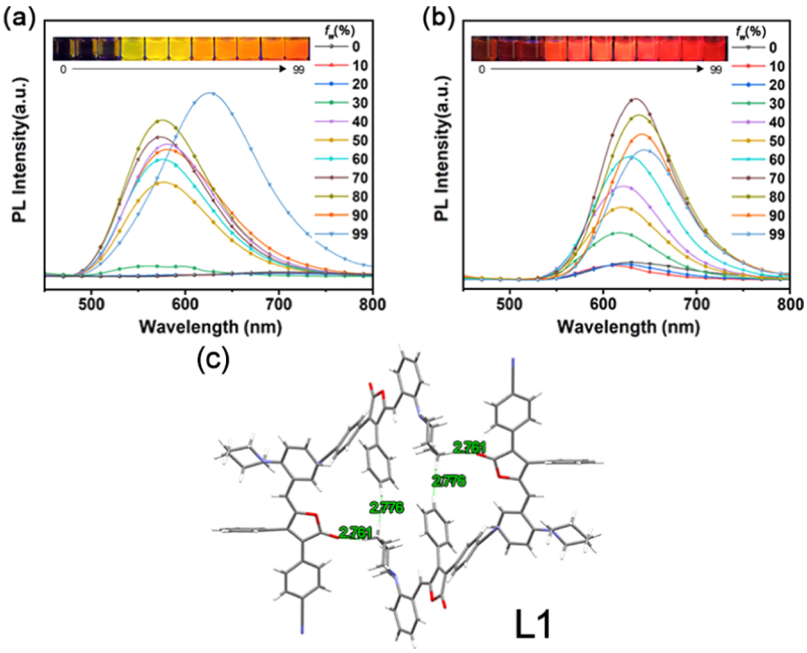

Figure 2. Emission spectra of **L1** (a) and **L4** (b) in DMSO-water of different compositions. (c) Two dimers of **L1** and intermolecular action. Inset: fluorescence images of **L1** and **L4** in DMSO with different water fractions under UV light (excited wavelength: 365 nm, 1×10^{-4} M).

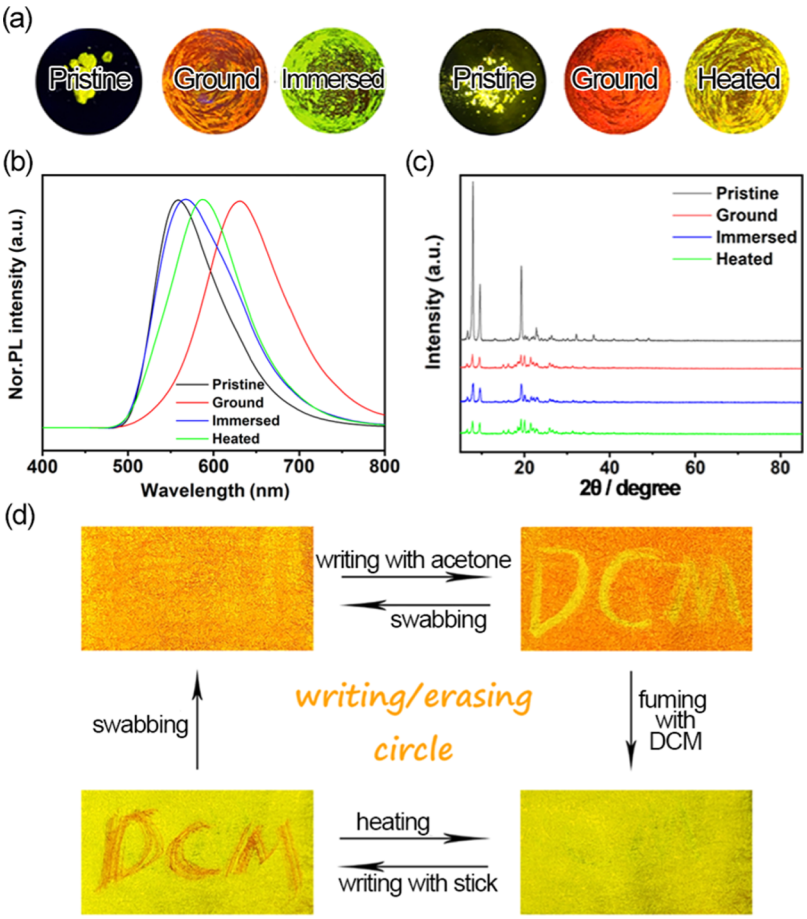

Figure 3. (a) Photographs of **L1** in different states under UV light. (b) Normalized solid-state emission spectra of **L1** in different states. (c) PXRD patterns of **L1**. (d) Photographs of **L1** in the writing/erasing cycle (excited wavelength: 365 nm).

to the absorption of the conjugated structure that had arisen from the ICT.[17] Among them, **L1** and **L4** had longer emission wavelengths. It indicated that introducing benzaldehyde with a stronger electron-donating group (piperidinyl) or a large site-

https://doi.org/10.1021/acsomega.1c06916
ACS Omega 2022, 7, 10994−11001

resistant group (diphenylamino) at the ortho-position into the OPBD unit could result in redshift of the emission maxima.[18,19]

The absorption spectra of the four compounds in various solvents are given in Figure S17. Next, we found that **L1**−**L4** have various maximum emission wavelengths (λ_{em}) in different solvents, which may be caused by the different degrees of ICT effect (Figures 1a,b, S17e,f).[20,21] Additionally, the different photoluminescence quantum yields of **L1** and **L4** in different solvents were measured (Table S2). Furthermore, the fluorescence intensity of **L1** and **L4** in different solvents decreased significantly as the polarity of solvent increased, which may be caused by the positive solvatokinetic effect.[22] To further understand the ICT effect of compounds, density functional theory calculations on electron cloud distribution and energy levels of **L1** and **L4** were done by using the B3LYP/6-31G (d) level of the theory embedded in the Gaussian 09 program. The computational data for highest occupied molecular orbital−lowest unoccupied molecular orbital (HOMO−LUMO) and energy gap are shown in Figure 1c. This result demonstrated that there was an increase in the energy gap and thus the bathochromic shift in the absorption wavelength, which agreed with the experimental spectra.[23−25]

The AIE phenomenon of **L1** and **L4** were demonstrated in a dimethyl sulfoxide (DMSO)/water mixture. As shown in Figure 2a, the emission intensity of **L1** was weak when it was in a solution state. As f_w was higher than 40%, it started to exhibit stronger emission intensity due to the formation of its aggregation. **L4** showed similar AIE behavior (Figure 2b). In contrast, when f_w was higher than 70%, the emission intensity gradually decreased. We hypothesized that the molecules might start agglomerating to form amorphous aggregates, which was harmful to the fluorescence emission.[26] On the contrary, **L2** and **L3** did not show an obvious AIE phenomenon as demonstrated in Figure S18. In addition, the photophysical properties of **L1** and **L4** were further investigated by femtosecond transient absorption (fs-TA) spectroscopy (Figure S19). According to the abovementioned TA results, **L1** and **L4** both showed fast and easy excited-state molecular motion, which suggested that nonradiative decay was predominant in the photophysical process of **L1** and **L4**. It might benefit their AIE phenomenon.[27−29] Further analysis of the single-crystal structure of the compounds helped to explain the mechanism of AIE. As shown in Figure 2c, the molecules of **L1** were held together with hydrogen bonding and packed loosely without obvious $\pi-\pi$ intramolecular interactions, which was beneficial for bright solid emission.

The fluorescence properties of **L1**-**L4** in the solid-state and the photographs of the solid powder under normal light and UV lamp were investigated (Figure S20). **L1** and **L4** showed MFC properties in response to external stimuli (Figures 3a,b, S21). Their solid emission spectra data were listed in Table S3. The λ_{em} of ground powder shifted to 628 nm. Following this, the ground sample could be reversed to its initial state by immersing with acetone. Meanwhile, heating the ground powder at 80 °C for 10 min could change its color from orange-red to yellow with a λ_{em} at 586 nm. This process could be repeated several times without fatigue. **L4** showed a similar mechanochromic behavior, but it could be restored to pristine condition (Figures S22 and S23).

PXRD patterns analysis was applied to get a deep insight into their mechanisms of mechanofluorochromism. The phase purity of the two compounds was confirmed by powder X-ray diffraction (PXRD). The peak positions of **L1** and **L4** between the experimental PXRD pattern and two simulated patterns are coincident with some differences existing in some peaks' intensities and widths (Figures S24 and S25).[30] As shown in Figure 3c, the pristine powder of **L1** showed intense and evident diffraction peaks indicating that it was a crystalline structure. The intensity of most diffraction peaks was greatly reduced or disappeared after grinding. It indicated that the ordered crystalline structure was destroyed into an amorphous state. When the ground powder was thermally treated or immersed with acetone, sharp diffraction peaks emerged again. As a result, it could be inferred that the mechanofluorochromism observed in **L1** is related to the change of morphology from crystalline to amorphous. Interestingly, the immersed sample showed a sharper peak than the thermally treated one. It implied that solvent immersion has a stronger effect on the crystallization of **L1** than thermal treatment. This also explained why the red amorphous powder cannot be completely restored to yellow crystals by heating.[31,32] The mechanism of mechanofluorochromism of **L4** was similar to **L1** by comparing the XRD curve results of both (Figure S21c). We further explored the reasons for their MFC behavior by analyzing the single-crystal structures of **L1**. Each molecule in **L1** is characterized by intermolecular C−H···π interactions (d = 2.776 Å, d = 4.984 Å, Figures S26 and S27) and C−H···O (d = 2.761 Å, d = 4.714 Å Figures S26 and S27) interactions by which they are held together. These weak intermolecular C−H···π interactions and C−H···O interactions resulted in a well-organized and loose pattern in **L1**, which could be easily disrupted by mechanical stimuli and lead to emission redshifts.[33]

The thermal stabilities of **L1** and **L4** were investigated by thermogravimetric analysis (TGA) and differential scanning calorimetry (DSC). As depicted in Figure S28 and Table S4, **L1** and **L4** are thermally stable in different states. The transition from a crystalline to an amorphous state upon grinding was further confirmed by DSC experiments. The DSC curves of **L1** (Figure S28) revealed that the melting point of **L1** was about 212 °C. The pristine sample of **L1** showed an endothermic transition peak at 205 °C, corresponding to the phase transition as opposed to cold crystallization. For the ground sample, the endothermic transition peak disappeared and showed new exothermal recrystallization peaks at 356.84 °C. After the ground samples were immersed in acetone, the endothermic transition peak at 205 °C reappeared without losing the exothermic recrystallization peak. However, the exothermic recrystallization peak disappears after heating of the ground **L1** sample, the DSC curve recovered similar to the pristine curve while the endothermic transition peak at 205 °C did not recover. It verified once more that solvent-induced recrystallization is better compared with heating.[34−36] The DSC curves of **L4** revealed that the pristine sample of **L4** showed an endothermic transition peak at 231.6 °C (Figure S28). For the ground sample, the endothermic transition peak moved to 230.5 °C. The endothermic transition peak recovered when the ground **L1** sample was heated or immersed in acetone.[37,38]

Based on their mechanochromic properties, we explored a practical application of **L1** in a rewritable paper. As shown in Figure 3d, the pristine powder of **L1** was applied on a piece of weighing paper. After the letters "DCM" were written on the paper using acetone as an ink. Then, the fluorescent letters could be erased by vaporing with dichloromethane (DCM) for a few seconds. Then the letters "DCM" could be written with a stick and be wiped off by swabbing or heating measures (Figure 3d).[39]

https://doi.org/10.1021/acsomega.1c06916
ACS Omega 2022, 7, 10994−11001

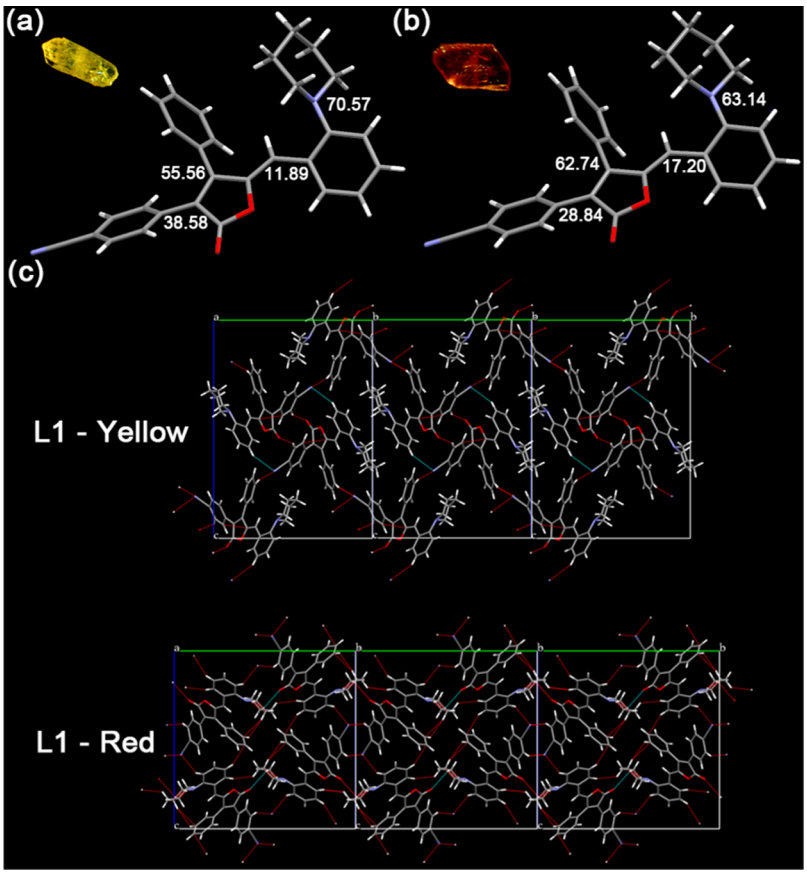

Figure 4. (a) Yellow single-crystal structure of **L1**. (b) Red single-crystal structure of **L1**. (c) Two different colors of crystal-packing diagram of **L1**. Inset: photographs of two different colors crystal of **L1** under normal light.

Interestingly, two types of single crystals of **L1** were obtained in the toluene solvent. One was yellow, the other was red (Figure 4a,b). Two detailed single-crystal analyses of **L1** were performed (Figure S29, Tables S5, and S6). At the single molecular level in the respective crystal, similar conformations were adopted. The four key dihedral angles are 38.58, 55.56, 11.89, and 70.57° in the yellow crystal, while they are 28.84, 62.74, 17.20, and 63.14° in the red crystal. The largest differences in the dihedral angles were less than 10°. Such differences indicated that the molecules in the red crystal adopted a more planar structure for three rings than the molecules in the yellow crystal. The single-molecule conformations for both crystals were not much different. As shown in Figure 4c, in the yellow crystal, the lactone ring was in close contact with the phenyl ring on the lactone ring of another molecule nearby. In contrast, in the red crystal, the lactone ring was in short contact with the piperidine ring of another molecule nearby. The *p*-cyanobenzene ring was surrounded by the phenyl ring on the lactone and the piperidine of a nearby molecule, as well as the phenyl ring with piperidine from another nearby molecule in the yellow crystal while it was in short contact with the phenyl ring with piperidine and the *p*-cyanobenzene ring of two nearby molecules. The slightly different conformations in the single-molecule structure and totally different molecular packing contributed to the different colors of both crystals.

As these molecules had basic groups, they may be acid-sensitive in solution or solid state.[36] Taking **L1** as an example, when the concentrations of trifluoroacetic acid (TFA) increased, the absorption band of **L1** around 425 nm in MeOH declined gradually, and a new absorption band at 350 nm appeared (Figure S30). Meanwhile, a blue shift was observed in the emission spectrum (Figure 5a). When the concentration of TFA increased from 0.67 to 21.32 mM, the fluorescence intensity at 688 nm decayed, and a new peak with maximum intensity at 480 nm formed. The fluorescence intensity was related to the TFA concentration over a certain range of TFA concentrations (Figure 5b). This phenomenon can be explained by the protonation of the piperidinyl group and the formation of salt. However, this salt was not stable, so the fluorescence change of **L1** gradually reversed as time passes. To make the process straightforward, under the UV light, an orange circle was drawn on paper by a drop of DCM containing **L1**. Subsequently, the orange circle was made blue within a few seconds by fuming with TFA vapor. Around 6 h later after stopping the fuming process, the blue circle recovered to orange (Figure 5c,d). The acidochromic property of **L1** inspired us to develop this compound as security inks. As depicted in Figure 5e, under normal light the letters "FIM" written with DCM solution of **L1** (10 mM) could disappear after fuming with TFA for a few seconds. After that, the letters could be revisualized by fuming with ammonia or without any treatment in air after 20 min. Moreover, the revisualized letters disappeared again by fuming with TFA (Figure 5e).[40]

CONCLUSIONS

In summary, inspired by the structure of TPB-1, we developed a "minus" strategy to design a new backbone of MSR materials, in which four compounds **L1**−**L4** were synthesized. Among them, **L1** and **L4** showed good AIE properties. In the solid state, their maximum emission generated redshift by grinding and could be

https://doi.org/10.1021/acsomega.1c06916
ACS Omega 2022, 7, 10994−11001

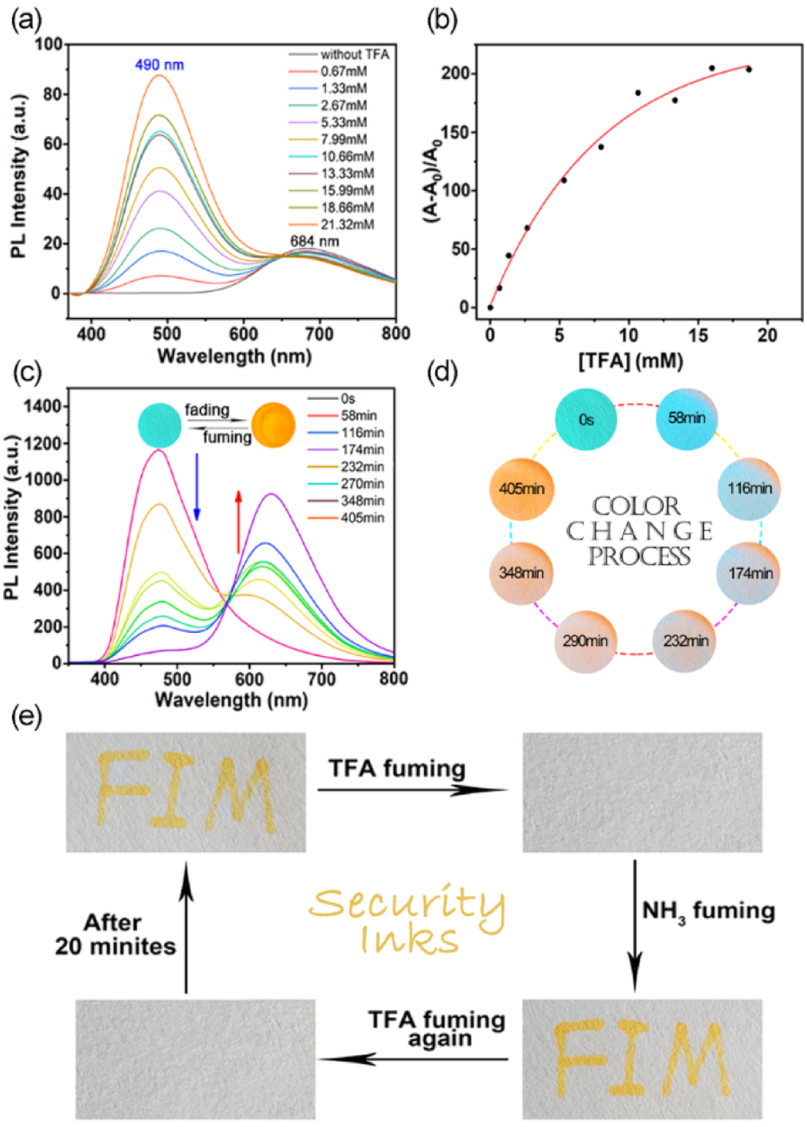

Figure 5. (a) Fluorescence spectra of **L1** (1×10^{-4} M) with different concentrations (0.67−21.32 mM) of TFA in the respective solutions of MeOH. (b) Fluorescence intensity of **L1** at 450 nm vs TFA concentration. (c) Fluorescence spectra of **L1** coated on filter paper (5×10^{-4} M) under TFA with different time points. (d) Color change process of **L1** filter paper (5×10^{-4} M) under TFA (13.33 M) with different time points. (e) Reversible color of **L1** switching by TFA (13.33 M) and NH_3 (14.79 M) exposure under normal light. Inset: images were taken under UV light.

recovered by solvent immersion or heating. PXRD curves revealed that the mechanochromic luminescent behavior was ascribed to the transformation from crystal form to an amorphous powder. In addition, **L1** showed the polymorph-dependent property and acidochromic property. This research provided a valuable reference for the design and development of new MSR materials.

■ ASSOCIATED CONTENT

Supporting Information

The Supporting Information is available free of charge at https://pubs.acs.org/doi/10.1021/acsomega.1c06916.

Crystallographic data for the L1 yellow crystal(CIF)

Crystallographic data for the L1 red crystal (CIF)

Synthesis routes, NMR data and MS spectra, crystallographic data, and additional data of compound **L1**−**L4** (PDF)

■ AUTHOR INFORMATION

Corresponding Author

Lijun Xie − *Fujian Provincial Key Laboratory of Screening for Novel Microbial Products, Fujian Institute of Microbiology, Fuzhou, Fujian 350007, PR China*; orcid.org/0000-0002-6503-6587; Email: lijunxie8224@outlook.com

Authors

Xiang Lin − *Fujian Provincial Key Laboratory of Screening for Novel Microbial Products, Fujian Institute of Microbiology, Fuzhou, Fujian 350007, PR China*

Xinli Wang − *Department of Oncology, Fujian Medical University Union Hospital, Fuzhou, Fujian 350001, PR China*

Renfu Li − *CAS Key Laboratory of Design and Assembly of Functional Nanostructures, and Fujian Key Laboratory of Nanomaterials, Fujian Institute of Research on the Structure of Matter, Chinese Academy of Sciences, Fuzhou, Fujian 350002, PR China*

https://doi.org/10.1021/acsomega.1c06916
ACS Omega 2022, 7, 10994−11001

Zexin Wang − *Fujian Provincial Key Laboratory of Screening for Novel Microbial Products, Fujian Institute of Microbiology, Fuzhou, Fujian 350007, PR China*
Wei Liu − *Fujian Provincial Key Laboratory of Screening for Novel Microbial Products, Fujian Institute of Microbiology, Fuzhou, Fujian 350007, PR China*
Liwei Chen − *Fujian Provincial Key Laboratory of Screening for Novel Microbial Products, Fujian Institute of Microbiology, Fuzhou, Fujian 350007, PR China*
Nannan Chen − *Fujian Provincial Key Laboratory of Screening for Novel Microbial Products, Fujian Institute of Microbiology, Fuzhou, Fujian 350007, PR China*
Shitao Sun − *Department of Medicinal Chemistry, School of Pharmaceutical Engineering, Shenyang Pharmaceutical University, Shenyang, Liaoning 110016, PR China*
Zhenli Li − *Department of Medicinal Chemistry, School of Pharmaceutical Engineering, Shenyang Pharmaceutical University, Shenyang, Liaoning 110016, PR China*
Jinle Hao − *Department of Medicinal Chemistry, School of Pharmaceutical Engineering, Shenyang Pharmaceutical University, Shenyang, Liaoning 110016, PR China*
Bin Lin − *Department of Medicinal Chemistry, School of Pharmaceutical Engineering, Shenyang Pharmaceutical University, Shenyang, Liaoning 110016, PR China;* orcid.org/0000-0003-2369-4765

Complete contact information is available at: https://pubs.acs.org/10.1021/acsomega.1c06916

Funding

This work was supported by the Strategic Priority Research Program of the CAS (XDB20000000), the NSFC of Fujian Province (no. 2020J06028) for L.X., the NSF of Fujian Province (no. 2020J011026) for X.W.

Notes

The authors declare no competing financial interest.

REFERENCES

(1) Abdurahman, A.; Wang, L.; Zhang, Z.; Feng, Y.; Zhao, Y.; Zhang, M. Novel triazole-based AIE materials: Dual-functional, highly sensitive and selective fluorescence probe. *Dyes Pigm.* **2020**, *174*, 108050.
(2) Yao, C.; Niu, C.; Na, N.; He, D.; Ouyang, J. Aggregation-induced emission compounds as new assisted matrices for laser desorption/ionization time-of-flight mass spectrometry. *Anal. Chim. Acta* **2015**, *853*, 375−383.
(3) Yan, L.; Zhang, Y.; Xu, B.; Tian, W. Fluorescent nanoparticles based on AIE fluorogens for bioimaging. *Nanoscale* **2016**, *8*, 2471−2487.
(4) Lu, X.-L.; Xia, M. Multi-stimuli response of a novel half-cut cruciform and its application as a security ink. *J. Mater. Chem. C* **2016**, *4*, 9350−9358.
(5) Han, J.; Sun, J.; Li, Y.; Duan, Y.; Han, T. One-pot synthesis of a mechanochromic AIE luminogen: implication for rewritable optical data storage. *J. Mater. Chem. C* **2016**, *4*, 9287−9293.
(6) Zhao, Z.; Lam, J. W. Y.; Tang, B. Z. Tetraphenylethene: a versatile AIE building block for the construction of efficient luminescent materials for organic light-emitting diodes. *J. Mater. Chem.* **2012**, *22*, 23726−23740.
(7) Zhao, F.; Chen, Z.; Fan, C.; Liu, G.; Pu, S. Aggregation-induced emission (AIE)-active highly emissive novel carbazole-based dyes with various solid-state fluorescence and reversible mechanofluorochromism characteristics. *Dyes Pigm.* **2019**, *164*, 390−397.
(8) Merkt, F. K.; Müller, T. J. J. Synthesis and electronic properties of expanded 5-(hetero)aryl-thien-2-yl substituted 3-ethynyl quinoxalines with AIE characteristics. *Sci. China Chem.* **2018**, *61*, 909−924.
(9) Huang, J.; Yang, X.; Li, X.; Chen, P.; Tang, R.; Li, F.; Lu, P.; Ma, Y.; Wang, L.; Qin, J.; Li, Q.; Li, Z. Bipolar AIE-active luminogens comprised of an oxadiazole core and terminal TPE moieties as a new type of host for doped electroluminescence. *Chem. Commun.* **2012**, *48*, 9586−9588.
(10) He, Y.; Li, Y.; Su, H.; Si, Y.; Liu, Y.; Peng, Q.; He, J.; Hou, H.; Li, K. An o-phthalimide-based multistimuli-responsive aggregation-induced emission (AIE) system. *Mater. Chem. Front.* **2019**, *3*, 50−56.
(11) Wang, Z.; Yu, F.; Chen, W.; Wang, J.; Liu, J.; Yao, C.; Zhao, J.; Dong, H.; Hu, W.; Zhang, Q. Rational Control of Charge Transfer Excitons Toward High-Contrast Reversible Mechanoresponsive Luminescent Switching. *Angew. Chem., Int. Ed.* **2020**, *59*, 17580−17586.
(12) Chen, J.; Xu, B.; Ouyang, X.; Tang, B. Z.; Cao, Y. Aggregation-Induced Emission of cis,cis-1,2,3,4-Tetraphenylbutadiene from Restricted Intramolecular Rotation. *J. Phys. Chem. A* **2004**, *108*, 7522−7526.
(13) Zeng, Q.; Li, Z.; Dong, Y.; Di, C. a.; Qin, A.; Hong, Y.; Ji, L.; Zhu, Z.; Jim, C. K. W.; Yu, G.; Li, Q.; Li, Z.; Liu, Y.; Qin, J.; Tang, B. Z. Fluorescence enhancements of benzene-cored luminophors by restricted intramolecular rotations: AIE and AIEE effects. *Chem. Commun.* **2007**, 70−72.
(14) Han, T.; Zhang, Y.; Feng, X.; Lin, Z.; Tong, B.; Shi, J.; Zhi, J.; Dong, Y. Reversible and hydrogen bonding-assisted piezochromic luminescence for solid-state tetraaryl-buta-1,3-diene. *Chem. Commun.* **2013**, *49*, 7049−7051.
(15) Ma, Z.; Wang, Z.; Meng, X.; Ma, Z.; Xu, Z.; Ma, Y.; Jia, X. A mechanochromic single crystal: turning two color changes into a tricolored switch. *Angew. Chem., Int. Ed.* **2016**, *55*, 519−522.
(16) Zhang, Y.; Xu, H.; Xu, W.; Zhang, C.; Shi, J.; Tong, B.; Cai, Z.; Dong, Y. Conformational sensitivity of tetraphenyl-1,3-butadiene derivatives with aggregation-induced emission characteristics. *Sci. China Chem.* **2019**, *62*, 1393−1397.
(17) Zhang, X.; Zhang, Y.; Zhang, H.; Quan, Y.; Li, Y.; Cheng, Y.; Ye, S. High Brightness Circularly Polarized Organic Light-Emitting Diodes Based on Nondoped Aggregation-Induced Emission (AIE)-Active Chiral Binaphthyl Emitters. *Org. Lett.* **2019**, *21*, 439−443.
(18) Lei, Y.; Liu, Y.; Guo, Y.; Chen, J.; Huang, X.; Gao, W.; Qian, L.; Wu, H.; Liu, M.; Cheng, Y. Multi-Stimulus-Responsive Fluorescent Properties of Donor-π-Acceptor Indene-1,3-dionemethylene-1,4-dihydropyridine Derivatives. *J. Phys. Chem. C* **2015**, *119*, 23138−23148.
(19) Zhang, L.; Hu, W.; Yu, L.; Wang, Y. Click synthesis of a novel triazole bridged AIE active cyclodextrin probe for specific detection of Cd2+. *Chem. Commun.* **2015**, *51*, 4298−4301.
(20) Li, K.; Cui, J.; Yang, Z.; Huo, Y.; Duan, W.; Gong, S.; Liu, Z. Solvatochromism, acidochromism and aggregation-induced emission of propeller-shaped spiroborates. *Dalton Trans.* **2018**, *47*, 15002−15008.
(21) Liang, X.; Zhang, Q. Recent progress on intramolecular charge-transfer compounds as photoelectric active materials. *Sci. China Mater.* **2017**, *60*, 1093−1101.
(22) Li, K.; Su, X.; Wang, Y.; Tao, F.; Cui, Y.; Zhang, H.; Li, T. D-π-A type barbituric derivatives: Aggregation induced emission, mechanofluorochromic and solvatochromic properties. *J. Lumin.* **2018**, *203*, 50−58.
(23) Schmitt, V.; Moschel, S.; Detert, H. Diaryldistyrylpyrazines: Solvatochromic and Acidochromic Fluorophores. *J. Org. Chem.* **2013**, *2013*, 5655−5669.
(24) Chen, S.; Liu, W.; Ge, Z.; Zhang, W.; Wang, K.-P.; Hu, Z.-Q. Dimethylamine substituted bisbenzocoumarins: solvatochromic, mechanochromic and acidochromic properties. *CrystEngComm* **2018**, *20*, 5432−5441.
(25) Naeem, K. C.; Subhakumari, A.; Varughese, S.; Nair, V. C. Heteroatom induced contrasting effects on the stimuli responsive properties of anthracene based donor-π-acceptor fluorophores. *J. Mater. Chem. C* **2015**, *3*, 10225−10231.
(26) Yang, C.-M.; Lee, I.-W.; Chen, T.-L.; Chien, W.-L.; Hong, J.-L. Enhanced emission of organic and polymeric luminogens containing

2,4,6-triphenylpyridine moieties: crystallization- and aggregation-enhanced emission. *J. Mater. Chem. C* **2013**, *1*, 2842−2850.
(27) Zhao, Z.; Zheng, X.; Du, L.; Xiong, Y.; He, W.; Gao, X.; Li, C.; Liu, Y.; Xu, B.; Zhang, J.; Song, F.; Yu, Y.; Zhao, X.; Cai, Y.; He, X.; Kwok, R. T. K.; Lam, J. W. Y.; Huang, X.; Lee Phillips, D.; Wang, H.; Tang, B. Z. Non-aromatic annulene-based aggregation-induced emission system via aromaticity reversal process. *Nat. Commun.* **2019**, *10*, 2952.
(28) Mei, J.; Hong, Y.; Lam, J. W. Y.; Qin, A.; Tang, Y.; Tang, B. Z. Aggregation-Induced Emission: The Whole Is More Brilliant than the Parts. *Adv. Mater.* **2014**, *26*, 5429−5479.
(29) Zhang, H.; Liu, J.; Du, L.; Ma, C.; Leung, N. L. C.; Niu, Y.; Qin, A.; Sun, J.; Peng, Q.; Sung, H. H. Y.; Williams, I. D.; Kwok, R. T. K.; Lam, J. W. Y.; Wong, K. S.; Phillips, D. L.; Tang, B. Z. Drawing a clear mechanistic picture for the aggregation-induced emission process. *Mater. Chem. Front.* **2019**, *3*, 1143−1150.
(30) Cai, K.; Zhao, N.; Zhang, N.; Sun, F.-X.; Zhao, Q.; Zhu, G.-S. A Homochiral Multifunctional Metal-Organic Framework with Rod-Shaped Secondary Building Units. *Nanomaterials* **2017**, *7*, 88.
(31) Ye, F.; Liu, Y.; Chen, J.; Liu, S. H.; Zhao, W.; Yin, J. Tetraphenylene-Coated Near-Infrared Benzoselenodiazole Dye: AIE Behavior, Mechanochromism, and Bioimaging. *Org. Lett.* **2019**, *21*, 7213−7217.
(32) Lu, T.; Wang, J.-Y.; Tu, D.; Chen, Z.-N.; Chen, X.-T.; Xue, Z.-L. Luminescent Mechanochromic Dinuclear Cu(I) Complexes with Macrocyclic Diamine-Tetracarbene Ligands. *Inorg. Chem.* **2018**, *57*, 13618−13630.
(33) Li, B.; He, T.; Shen, X.; Tang, D.; Yin, S. Fluorescent supramolecular polymers with aggregation induced emission properties. *Polym. Chem.* **2019**, *10*, 796−818.
(34) Gundu, S.; Kim, M.; Mergu, N.; Son, Y.-A. AIE-active and reversible mechanochromic tetraphenylethene-tetradiphenylacrylonitrile hybrid luminogens with re-writable optical data storage application. *Dyes Pigm.* **2017**, *146*, 7−13.
(35) Li, H.; Zhang, X.; Chi, Z.; Xu, B.; Zhou, W.; Liu, S.; Zhang, Y.; Xu, J. New thermally stable piezofluorochromic aggregation-induced emission compounds. *Org. Lett.* **2011**, *13*, 556−559.
(36) Liu, C.; Luo, H.; Shi, G.; Yang, J.; Chi, Z.; Ma, Y. Luminescent network film deposited electrochemically from a carbazole functionalized AIE molecule and its application for OLEDs. *J. Mater. Chem. C* **2015**, *3*, 3752−3759.
(37) Mao, Z.; Yang, Z.; Mu, Y.; Zhang, Y.; Wang, Y.-F.; Chi, Z.; Lo, C.-C.; Liu, S.; Lien, A.; Xu, J. Linearly Tunable Emission Colors Obtained from a Fluorescent-Phosphorescent Dual-Emission Compound by Mechanical Stimuli. *Angew. Chem.* **2015**, *127*, 6368−6371.
(38) Takahashi, S.; Nagai, S.; Asami, M.; Ito, S. Two types of two-step mechanochromic luminescence of phenanthroimidazolylbenzothiadiazoles. *Mater. Adv.* **2020**, *1*, 708−719.
(39) Ma, Y.; Zhang, Y.; Kong, L.; Yang, J. Mechanoresponsive Material of AIE-Active 1,4-Dihydropyrrolo[3,2-b]pyrrole Luminophores Bearing Tetraphenylethylene Group with Rewritable Data Storage. *Molecules* **2018**, *23*, 3255.
(40) Li, Y.; Wang, X.; Zhang, L.; Liu, L.; Wang, Q.; Lu, H.; Zhao, X. Remarkable solid-state fluorescence change from the visible to the near-infrared region based on the protonation/deprotonation of an AIEgen. *Mater. Chem. Front.* **2020**, *4*, 3378−3383.

https://doi.org/10.1021/acsomega.1c06916
ACS Omega 2022, 7, 10994−11001